IEEE Access
Multidisciplinary | Rapid Review | Open Access Journal

Received June 9, 2022, accepted June 16, 2022, date of publication June 21, 2022, date of current version June 24, 2022.

*Digital Object Identifier 10.1109/ACCESS.2022.3184778*

# Miniaturized Antenna for High Data Rate Implantable Brain-Machine Interfaces

**NAEEM ABBAS[1], SYED AHSON ALI SHAH[2], (Graduate Student Member, IEEE), ABDUL BASIR[2], (Member, IEEE), ZUBAIR BASHIR[1], ADEEL AKRAM[1], AND HYOUNGSUK YOO[2], (Senior Member, IEEE)**

[1]ACTSENA Research Group, Telecommunication Engineering Department, University of Engineering and Technology Taxila, Taxila 47050, Pakistan
[2]Department of Electronic Engineering, Hanyang University, Seoul 04763, South Korea

Corresponding author: Hyoungsuk Yoo (hsyoo@hanyang.ac.kr)

This work was supported by the Institute for Information & Communications Technology Promotion (IITP) funded by the Korean Government through the Ministry of Science and ICT and Future Planning (MSIP) under Grant 2022-0-00310.

**ABSTRACT** Technological advancements in medical care have necessitated the development of efficient and miniaturized implantable medical devices. This paper presents an ultra-wide-band implantable antenna for use in scalp-based biomedical applications covering the industrial, scientific, and medical (ISM) (2.4−2.48 GHz) band. The proposed antenna is mounted on a 0.1−mm thick liquid crystalline polymer (LCP) Roger ULTRALAM ($\tan\delta = 0.0025$ and $\varepsilon_r = 2.9$), serving as a dielectric material for both the superstrate and substrate layers. LCP materials are widely used in manufacturing electronic devices owing to their desirable properties, including flexibility, conformable structure, and biocompatibility. To preserve the capability of an electrically small radiator and achieve optimum performance, the proposed antenna is designed to have a volume of 9.8 $mm^3$ (7 mm × 7 mm × 0.2 mm). The addition of a shorting pin and open-ended slots in the radiating patch, and close-ended slots in the ground plane facilitates antenna miniaturization, impedance matching, and bandwidth expansion. Notably, the antenna exhibits a peak gain of −20.71 dBi and impedance-matched bandwidth of 1038.7 MHz in the ISM band. Moreover, the antenna is safe to use according to the IEEE C905.1-2005 safety guidelines based on low specific absorption rates. To evaluate the performance of the implantable antenna, finite-element simulation was performed in homogeneous and heterogeneous environments. For validation, measurements were performed in a minced pork-filled container. The simulation results are consistent with the measurements. In addition, a link budget analysis is performed to confirm the robustness and reliability of the wireless telemetric link and determine the range of the implantable antenna.

**INDEX TERMS** Implantable antenna, high gain, novel shaped, specific absorption rate, ultra-wide band.

## I. INTRODUCTION

Implantable medical devices (IMDs) enable early diagnosis of human diseases and play a significant role in several biomedical applications, such as intracranial pressure detection, glucose monitoring, capsule endoscopy, and cardiac pacemakers [1], [2]. These devices can be used to continuously monitor human health and facilitate the exchange of various physiological information using an external controller [3]. To integrate wireless capabilities in an IMD, a small and efficient implantable antenna that enables the device to establish a real-time biotelemetric link is required [4] with an on-body wearable and body-centric devices with high-performance antenna systems [5]–[7]. Medical professionals can remotely analyze this information and provide necessary treatment using high data rate MIMO-based biomedical devices [8]–[10], thereby improving the quality of life.

Several frequency bands are regulated by the Federal Communications Commission (FCC) for use in biomedical applications, including medical implant communications service (MICS, 402 − 405 MHz), improved MICS, called the medical device radio communication Service (MedRadio, 401 − 406 MHz) [11], and industrial, scientific, and medical

The associate editor coordinating the review of this manuscript and approving it for publication was Junhua Li.

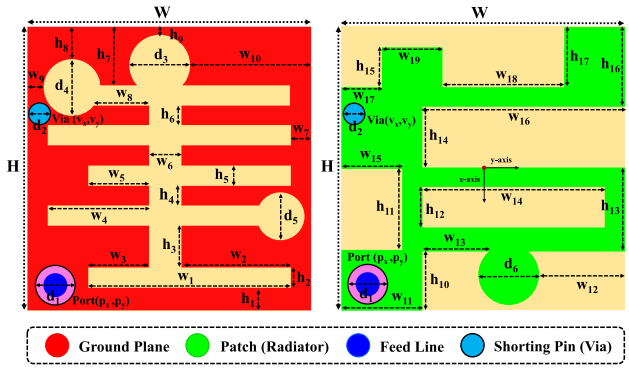


**FIGURE 1.** Configuration of the proposed implantable antenna.

(ISM, 433 − 438 MHz; 902 − 928 MHz; 2.4 − 2.48 GHz; and 5.725 − 5.875 GHz) bands. To extend the device lifetime and battery energy, a sleep-wakeup mode is utilized at 2.45 GHz [12] as the IMDs consume less power in the sleep mode than in the wake-up mode [13]. Moreover, the ISM band of 2.45 GHz is primarily used in biomedical applications owing to the increased radiated power at high frequencies [14].

Typically, the implantable antennas are placed inside the human body, which is heterogeneous and lossy by nature. The differences in the permittivity and conductivity values of different human tissues impose serious challenges on implantable antennas face, such as impedance mismatching and detuning effects [15]. To address these problems, an implantable antenna with wide bandwidth is preferred. Moreover, several additional challenges must be addressed, following the guidelines reported in [16], to develop an implantable antenna, including size restriction, bandwidth, biocompatibility, patient safety, and reliable telemetry.

Recently, numerous implantable antennas have been developed for biomedical applications. A multiple-input multiple-output (MIMO) antenna with an electromagnetic bandgap structure was proposed in [17]. Despite the isolation attained by the EBGs and large structural dimensions ($18.5 \times 18.5 \times 1.27$ mm$^3$), the antenna exhibited a simulated bandwidth of 440 MHz and a peak gain of −15.18 dBi in the ISM band. Moreover, the MIMO technique is an unrealistic approach to IMD owing to its limited power resources. An implantable antenna for the MedRadio band was designed in [18]. However, the structure had a large area of 66.89 mm$^2$ and exhibited a comparatively low bandwidth (139.6 MHz). A circularly polarized (CP) implantable antenna was designed at the 2.4 GHz ISM band for cardiac pacemaker applications [19]. Although the gain (−15.87 dBi) and bandwidth (890 MHz) were satisfactory, the antenna had a large footprint ($40 \times 40 \times 1.27$ mm$^3$). In [20], a triple-band implantable antenna for multiple biomedical applications was proposed in the ISM (915 MHz and 2.45 GHz) and midfield (1824 − 1980 MHz) bands. However, it exhibits lower bandwidths and gain values in the ISM and midfield bands. Similarly, a dual-band implantable antenna operating in the

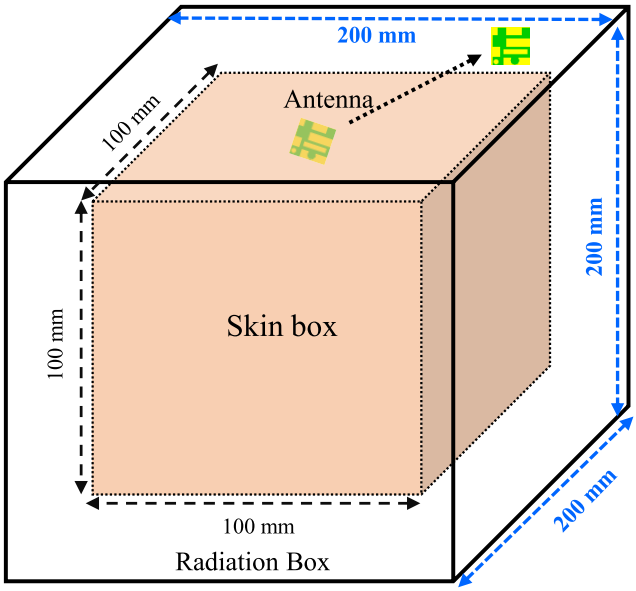


**FIGURE 2.** Simulation setup for the proposed antenna.

ISM and MedRadio bands was proposed in [21]. The antenna offered an unsatisfactory bandwidth and had a large footprint. In [22], a single-band implantable antenna operating in the ISM (2.4 − 2.48 GHz) band was designed for glucose monitoring. Although the gain (−17 dBi) was high, the structure had a large volume (91.7575 mm$^3$) and a lower bandwidth (300 MHz). A novel shaped antenna operating in the ISM and MICS bands was proposed for pacemakers [14]. However, the antenna had a complex geometry, large dimensions, and low gain values. In [23], a flexible slot antenna integrated with a metamaterial (MTM) array was proposed for biotelemetry applications. To enhance the gain of the antenna, an MTM array with epsilon very large (EVL) properties was utilized in the superstrate of the antenna. Although the EVL-based MTM array improved the gain by 3 dBi, it increased the overall volume of the antenna. Similarly, in [24], a CP implantable microstrip patch antenna (MPA) operating in the ISM band was presented. Two high-order degenerate modes were excited in the MPA to generate CP radiating waves at low-gain values. In addition to the complex geometry of the antenna, its dimensions were large. These observations indicate that antennas developed for biomedical applications at various frequencies have several limitations and are unsuitable for use in IMDs. Therefore, further research is required to develop an efficient implantable antenna with a small volume, high gain, large bandwidth, low SAR, and reliable telemetric capability.

This study developed an ultrawideband implantable antenna for biotelemetric IMDs implanted under the scalp. The proposed antenna has a volume of 9.8 mm$^3$ and is characterized by its single operating mode: data telemetry in the ISM band (2.4 − 2.48 GHz). To achieve optimum performance on a miniature structure comprising a radiating element and ground plane embedded in the LCP Rogers ULTRALAM substrate and superstrate layers, several

**TABLE 1. Comparison with the previous work.**

| Ref | Volume [$mm^3$] | Frequency [GHz] | SAR (W/Kg) 1-g | Bandwidth [MHz] | Gain [dBi] | Dielectric Material | Patch Shape | Shorting Pin |
|---|---|---|---|---|---|---|---|---|
| [1] | 17.15 | 0.402<br>1.6<br>2.45 | 588<br>441<br>305 | 148<br>171<br>219 | −30.5<br>−22.6<br>−18.2 | Rogers RT/ Duroid 6010 | Zig Zag | Yes |
| [19] | 21 | 2.45 | 217.849 | 890 | −20.47 | Rogers RT/ Duroid 6010 | Zig Zag | No |
| [20] | 66.41 | 2.45<br>2.8 | 217 | 80<br>115 | −10.3<br>−10.3 | TMM 13i | Zig Zag | Yes |
| [21] | 31.5 | 2.45 | 778.1 | 246 | −21.2 | Rogers 6010 | Spiral | Yes |
| [22] | 91.75 | 2.45 | – | 300 | −17 | Rogers 3210 | Circular | No |
| [25] | 52.5 | 0.405<br>0.915<br>4.45 | 665.35<br>837.69<br>759.72 | 64<br>91<br>105 | −40.8<br>−32.9<br>−22.3 | Rogers 6010 | Zig Zag | Yes |
| [26] | 67.8 | 2.45 | 238.9 | 980 | −19.2 | Rogers 3010 | Rectangular | Yes |
| [27] | 161.29 | 2.45 | 213 | 190 | −22 | Rogers 3010 | Rectangular | No |
| [28] | 434.65 | 2.45 | 1.5 | 440 | −15.8 | Rogers 6010LM | Spiral | Yes |
| [29] | 254 | 2.45 | 382 | 60 | −15 | Roger 3210 | Pi-Shape | Yes |
| [30] | 203.6 | 0.915 | 679.797 | 40 | −16 | Rogers RO3010 | Meandered | Yes |
| [31] | 127 | 2.45 | 254.74 | 390 | −17.2 | Rogers 3010 | wafĭňĆe | No |
| Proposed Work | 9.8 | 2.45 | 289.76 | 1038.7 | −20.71 | Ultralam | Square | Yes |

miniaturizing techniques were employed in the design. In addition to the increment in the electrical length, impedance improvement and bandwidth extension at the desired frequency band are achieved by the addition of circular slots, rectangular open-ended slots, and a shorting pin. First, the proposed antenna was designed and analyzed using a homogeneous skin phantom (HSP) with dimensions of 100 mm × 100 mm × 100 mm. Next, the performance of the proposed antenna was validated in a heterogeneous medium containing multiple human body tissues. To validate the computational results, the fabricated prototype of the implantable antenna was tested in a human tissue-mimicking realistic environment comprising container-filled minced pork. Notably, the structure attained an impedance-matched bandwidth of 1038.7 MHz and a peak gain of −20.71 dBi with omnidirectional radiation characteristics. The SAR safety analysis revealed that the antenna is safe to use. A communication range of 12 m can be reliably achieved at a bitrate of 200 kbps owing to its high-gain performance, as determined by the link budget calculations. Table 1 lists the results of the comparative analysis between the proposed antenna and those proposed in previous studies, indicating the superiority of the proposed antenna over the other antennas in terms of structural simplicity, volume, antenna material, bandwidth, gain, and SAR patient safety.

The remainder of this paper is organized as follows. Section II describes the methodology and design of the antenna, and the parametric analysis. Section III presents the results and discussion in terms of antenna performance. Section IV presents a link budget analysis, and Section V concludes the study.

## II. METHODOLOGY

This study aims to develop an ultra-wideband implantable antenna for scalp-based biomedical applications that performs effective biotelemetric communication with an external controller and satisfies several requirements for its implantation inside the human body, such as small size, biocompatibility, good radiation characteristics, and patient safety.

### A. ANTENNA DESIGN

Fig. 1. shows the configuration of the proposed miniaturized implantable antenna with the dimensions of 7 mm × 7 mm × 0.2 mm. The antenna comprises a central radiator, ground plan, shorting pin, superstrate, and substrate. As is evident from the figure, several rectangular and circular open-ended slots are etched on both the ground plane and radiator of the rectangular patch antenna to achieve bandwidth enhancement, elevated gain, and miniaturization.

To achieve biocompatibility, Roger ULTRALAM 3850HT ($\tan\delta = 0.0025$ and $\varepsilon_r = 2.9$) was used as the dielectric material for the substrate. The ground plane was used as the lower conductive layer of the substrate, whereas the upper layer served as the main radiator. A superstrate layer of the same material was used to insulate the antenna and eliminate short circuits induced by lossy human tissues. The thickness of both the superstrate and substrate was restricted to 0.1 mm to reduce the overall volume. Roger ULTRALAM is a liquid crystalline polymer (LCP) material that provides constant electrical properties for tightly controlled impedance matching and is used to manufacture electronic devices [32]. Owing to its minimal dielectric and tangent losses, Roger ULTRALAM is preferred for biomedical applications [33]. A 50Ω coaxial feed port with a diameter of 0.6 mm was used to excite the antenna. The parameters of the proposed ultra-compact implantable antenna are listed in Table 2. These parameters are obtained by optimizing the radiating structure to operate at the central frequency of 2.45 GHz with a compact footprint.

**TABLE 2. Parameters of the proposed antenna. (Units: *mm*.)**

| Parameters | Values | Parameters | Values | Parameters | Values |
|---|---|---|---|---|---|
| $W$ | 7.0 | $w_{15}$ | 1.5 | $h_{12}$ | 1.0 |
| $H$ | 7.0 | $w_{16}$ | 5.0 | $h_{13}$ | 2.0 |
| $w_1$ | 5.0 | $w_{17}$ | 1.0 | $h_{14}$ | 1.5 |
| $w_2$ | 2.7 | $w_{18}$ | 3.0 | $h_{15}$ | 1.0 |
| $w_3$ | 1.5 | $w_{19}$ | 1.5 | $h_{16}$ | 2.0 |
| $w_4$ | 2.5 | $h_1$ | 0.5 | $h_{17}$ | 1.5 |
| $w_5$ | 1.5 | $h_2$ | 0.5 | $d_1$ | 1.0 |
| $w_6$ | 0.8 | $h_3$ | 1.0 | $d_2$ | 0.6 |
| $w_7$ | 0.5 | $h_4$ | 0.5 | $d_3$ | 1.6 |
| $w_8$ | 1.24 | $h_5$ | 0.5 | $d_4$ | 1.5 |
| $w_9$ | 0.45 | $h_6$ | 0.5 | $d_5$ | 1.3 |
| $w_{10}$ | 2.9 | $h_7$ | 1.5 | $d_6$ | 1.64 |
| $w_{11}$ | 2.0 | $h_8$ | 0.8 | $p_x$ | 2.85 |
| $w_{12}$ | 2.0 | $h_9$ | 0.2 | $p_y$ | −2.85 |
| $w_{13}$ | 1.64 | $h_{10}$ | 1.5 | $v_x$ | −1.4 |
| $w_{14}$ | 4.5 | $h_{11}$ | 2.0 | $v_y$ | −3.18 |

### B. SIMULATION SETUP

The initial simulation setup for the designed antenna is illustrated in Fig. 2. The proposed antenna was simulated in a HSP with dimensions of 100 mm × 100 mm × 100 mm in Ansoft HFSS. The antenna was placed at the center of a single-layer HSP model enclosed by an airbox that served as a radiation boundary. According to [22], the dielectric properties of human tissues are dependent on the operating frequency, which was 2.45 GHz in this study. A relative permittivity ($\varepsilon_r$) of 38 and an electrical conductivity of 1.46 S/m at 2.45 GHz were assigned to the HSP to mimic human skin tissue.

### C. DESIGN STEPS

The antenna was developed in four steps to obtain optimum performance at the required resonance band (Fig. 3). Several rectangular slots and cuts were added to the patch and the ground plane to extend the electrical length of the antenna and achieve compactness.

A comparison of the reflection coefficients ($S_{11}$) for the different design steps utilized to develop the proposed wideband implantable antenna is shown in Fig. 4. The resonant frequency is in the 4.2 GHz region in the initial phase, with poor impedance-matching characteristics ($S_{11} > -10$ dB). At this stage, the frequency can easily be shifted to the lower region by increasing the dimensions of the antenna. However, large antennas are unsuitable for biomedical applications. Therefore, a few rectangular slots were created in the patch and ground plane to achieve the desired resonance. Despite having identical dimensions, an elongated path is established for the currents to flow over the surface of the radiating patch and ground plane, thereby shifting the frequency to a lower band [34]. This phenomenon can be observed from the $S_{11}$ graphs, which exhibit a dual resonance at 1.2 and 3.4 GHz achieved in the second and third steps with similar impedance-matching features. In the final design process, more slots were added to the center of the radiating patch.The insertion of slots creates small capacitive gaps on the radiator and ground plane, which improve impedance-matching

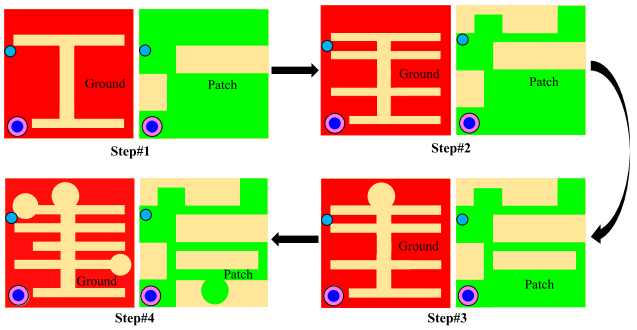


**FIGURE 3. Designing steps of the proposed antenna.**

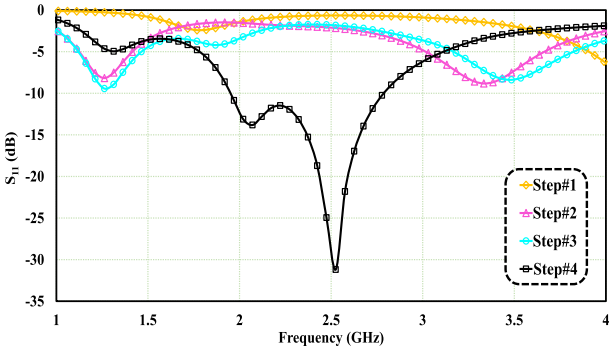


**FIGURE 4. Return loss ($S_{11}$) of the successive designing steps.**

characteristics. Moreover, parasitic capacitance aids in shifting the resonance to the lower side of the frequency spectrum [35]. Notably, the proposed antenna exhibited a perfectly matched impedance with minimal reflections at the desired 2.45 GHz ISM band, covering a large bandwidth of 874.3 MHz (from 1945 MHz to 2829 MHz).

### D. PARAMETRIC ANALYSIS

The performance of an antenna is greatly influenced by the size and length of various parameters. Therefore, a parametric analysis was performed to optimize and tune the final antenna design. A few essential parameters were considered for performance evaluations, such as slot $w_1$ in the ground plane, circular cut with a diameter ($d_6$) and slot $w_{15}$ in the radiating element. Furthermore, the effect of the shorting position was investigated. In the simulation environment, the values of the critical parameters were varied to analyze their impacts on $S_{11}$, which was used to fine-tune the antenna.

#### 1) EFFECT OF VARYING THE PARAMETER $w_1$

Fig. 5 shows the effect of the variation in the slot parameter $w_1$ on the reflection coefficient. Increasing the value from 4 mm to 5.5 mm in steps of 0.5 mm, the resonance frequency is shifted towards the lower band. Further increments in $w_1$ cause the close-ended slot to become open-ended and split the current path in two directions near the feed port on the ground plane−one in the upward direction towards the shorting pin and the other in the lower-right direction.

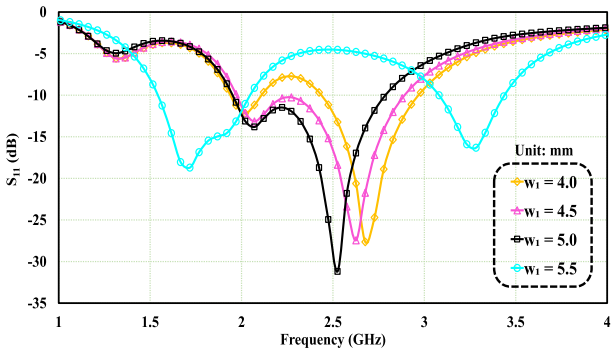


**FIGURE 5.** Effect of Variation in slot length ($w_1$) on the return loss ($S_{11}$).

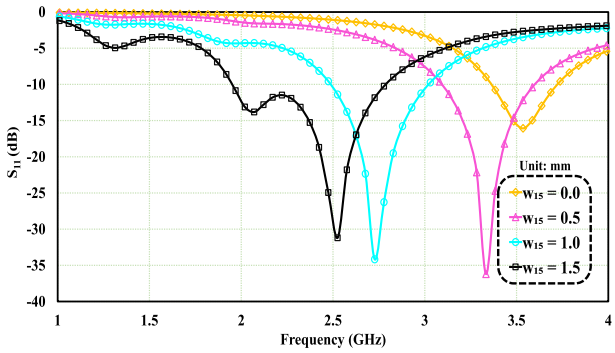


**FIGURE 7.** Effect of change in width of side strip ($w_{11}$) on the return loss ($S_{11}$).

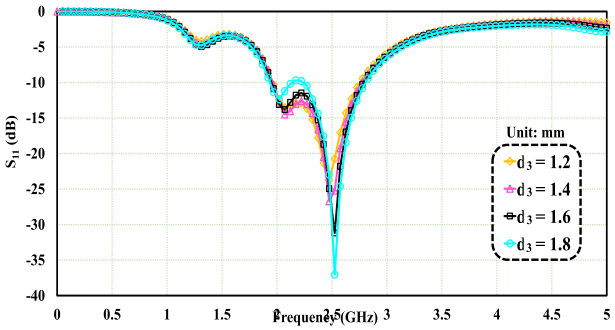


**FIGURE 6.** Effect of change in diameter of slot ($d_3$) on the return loss ($S_{11}$).

When $w_1$ is extended to 5.5 mm, parameter $w_1$ vanishes. The two resonances occur at 1.7 GHz and 3.3 GHz in this case, implying that the length $w_1$ exerts a more significant influence on impedance matching and antenna tuning in the appropriate frequency band.

#### 2) EFFECT OF VARYING THE PARAMETER $d_3$

Fig. 6 shows the effect of the circular cut ($d_3$) on $S_{11}$, which ranges from 1.2 mm to 1.8 mm. Evidently, increasing the value of $d_3$ results in improved impedance matching. However, at $d_3 = 1.8$ mm, the resonance splits into two bands, eliminating the wideband characteristics of the proposed antenna. Therefore, the value of $d_3$ is set to 1.6 mm to obtain ultra-wide bandwidth.

#### 3) EFFECT OF VARYING THE PARAMETER $w_{15}$

The width of the rectangular cut $w_{15}$ has a significant effect on the impedance matching and stability of the designed antenna. Fig. 7 shows the effect of the variation in the width of the side strip $w_{15}$ on $S_{11}$ of the antenna. First, return loss is observed without the side strip. The antenna resonates at 3.5 GHz, with a dip of $<-10$ dB in the $S_{11}$. Subsequently, a strip with a width in the range of $0.5-1.5$ mm is added. At the lower values of the strip $w_{15}$, the desired band is not achieved, and $S_{11}$ exhibits a peak dip at 3.3 GHz. By increasing the size of $w_{15}$, impedance matching is gradually improved, and the frequency is shifted to the lower side of the spectrum. Further increments in the width of the strip elongated the current path, and the required frequency band was achieved by setting $w_{15}$ to 1.5 mm.

#### 4) EFFECT OF VARYING THE SHORTING PIN LOCATION

The effect of the shorting pin on the performance of the proposed antenna was also analyzed at four different locations (Fig. 8). Evidently, the shorting pin facilitates impedance matching and tuning of the implantable antenna. The antenna is completely mismatched when the shorting pin is placed near the feed port at the location $P_1$. The currents experience a small path on the main radiator shorted with the ground, causing a poor resonance at 4.5 GHz. When the shorting pin was moved to the location $P_2$, multiple current paths were created, causing weak ($S_{11} > -10$ dB) resonances at multiple undesired frequencies. At $P_3$, where the shorting pin is moved to the upper-right corner of the antenna, dual bands are produced at 900 MHz and 3.15 GHz. Finally, the shorting pin is optimized at position $P_4$ where the antenna exhibits perfectly matched impedance and wideband characteristics at the desired frequency of 2.45 GHz. Generally, a shorting pin is added in the structure to short the radiator with the ground plane. Typically, the shorting pin is smaller in radius, which is usually between 0.1 to 0.3 mm. This radius is taken according to the trace width on the radiator. As long as the diameter of a shorting pin is not greater than the maximum width of the trace on which it is added, there is no affect on the $S_{11}$ and gain of the implantable antenna. However, when the diameter of shorting pin is increased in such a way that it occupies two or more traces, there is effect on the $S_{11}$ and gain of the implantable antenna. As more traces on the radiator are shorted with the ground plane, the frequency response is deteriorated. Therefore, in this study, the diameter of a shorting pin is restricted to 0.6 mm in diameter so that it can short a single trace on the radiator with the ground plane.

### E. FABRICATION AND MEASUREMENTS

As previously mentioned, initial simulations were performed in FEM-based homogeneous model. To further inspect the sensitivity of antenna, numerical computations were

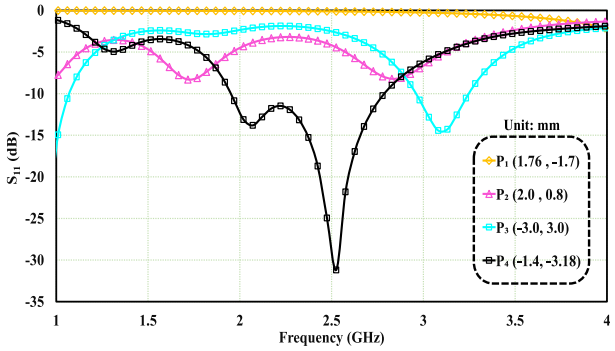


**FIGURE 8.** Effect of change in the position of shorting pin (via) on return loss ($S_{11}$).

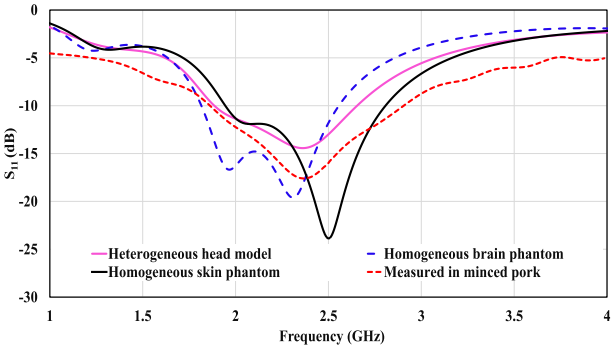


**FIGURE 10.** return loss $S_{11}$ of the proposed antenna in different implant situations.

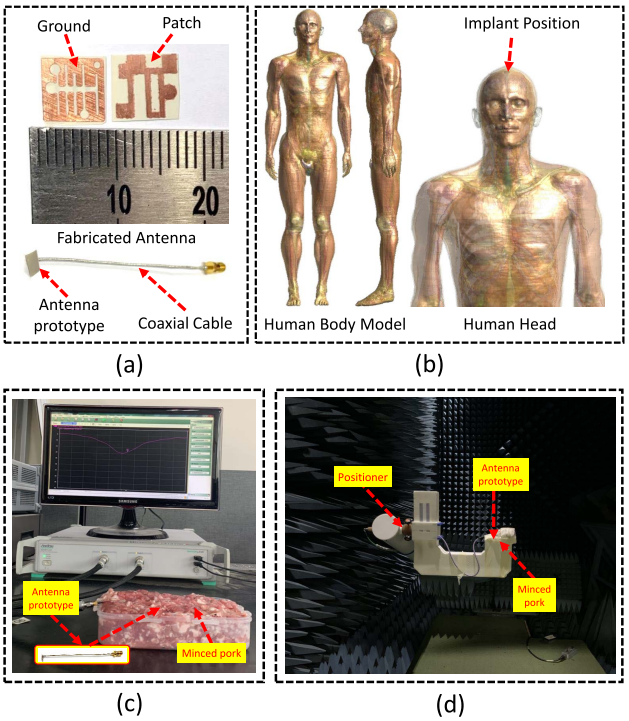


**FIGURE 9.** (a) Fabricated Antenna prototype. (b) 3-D human body model and antenna implant position. (c) Return loss $S_{11}$ measurement setup in minced pork meat. (d) Radiation chamber to measure of radiation efficiency of the proposed antenna in minced pork meat.

conducted in the heterogeneous environment, such as head model comprised of multiple human tissues. In both cases, the antenna was implanted at depth of d = 12 mm. For experimentation, the fabricated prototype of antenna is developed using photolithographic technique in which the metalizations of the slots and cuts on the radiating element and ground planes were chemically etched off. Afterward, the soldering process was adopted to connect an SMA cable with the fabricated antenna. To evaluate the simulated attributes, the real-time performance was analyzed by measuring the reflection coefficient and radiation pattern in a minced pork emulating human biological tissues. The realistic duke model, fabricated antenna, and measurement setup are shown in Fig. 9.

## III. RESULTS AND DISCUSSION

The performance of the proposed implantable antenna was analyzed with respect to the reflection coefficient, far-field gain pattern, patient safety, and link budget. $|S_{11}|$ of the proposed antenna in a HSP, homogeneous brain model, realistic heterogeneous head model, and minced pork are compared in Fig. 10. Evidently, that the proposed antenna exhibits ultra-wideband performance at a resonant frequency of 2.45 GHz. The antenna offers a $-10$ dB bandwidth of 874 MHz (1.945 $-$ 2.829 GHz) and 792 MHz (1.801 $-$ 2.593 GHz). A slight shift in the frequency spectrum and dip in the return loss were observed because of the high permittivity of the brain compared to the skin. The antenna exhibits a band coverage of 801.2 MHz (1.881 $-$ 2.6817 GHz) in a heterogeneous head environment. The complex and diverse electrical properties existing in a realistic human head model cause a slight shift in resonant frequency. The antenna offers a $-10$ dB bandwidth of 1038.7 MHz (1.868 $-$ 2.925 GHz) in this realistic environment. Owing to fabrication tolerances and human procedural errors, a slight shift in the simulated and measured values was observed. However, these effects are negligible, as the antenna covers the desired band (2.45 GHz) in all scenarios.

The current distribution in the proposed antenna in the four successive phases is shown in Fig. 11. $\theta = 0°$ and 180°, the currents flow primarily around the feed point; however, the polarity is opposite in both cases. The flow of currents from the feed towards the shorting pin on the ground plane increases at $\theta = 90°$ indicating that the charge is coupled between the ground plane and radiator, thereby elongating the current path. The same phenomenon was observed at $\theta = 270°$ wherein the currents flowed in the opposite direction to that at $\theta = 90°$. Notably, a half-wavelength dipole mode was observed at 2.45 GHz in all cases.

Owing to signal transmission through lossy tissues in the human body, the gain of implantable antennas is substantially lower than that of free-space antennas. Fig. 12 shows

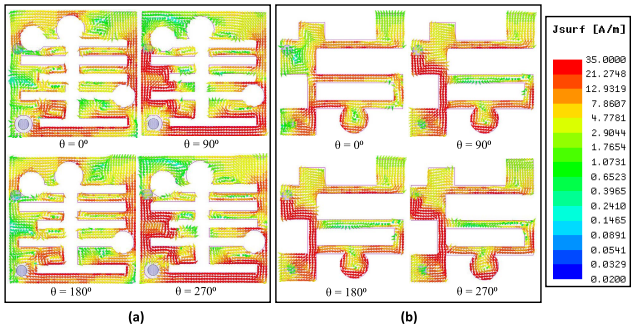


**FIGURE 11.** Current distribution effect on the proposed antenna. (a) Ground plane. (b) Radiating element.

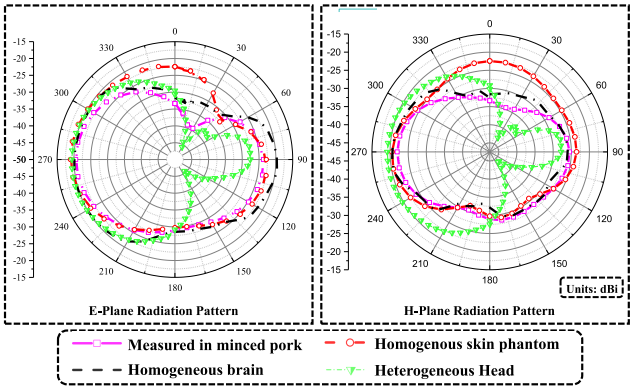


**FIGURE 12.** simulated and measured radiation efficiency of the proposed antenna.

the radiation patterns of the proposed implantable antenna. The H-plane and E-plane radiation patterns of the designed antenna depend on the human body tissue in which the antenna is implanted [34]. Realized peak gain values of −19.06, −19.57, −19.36, and −20.71 dBi were attained in the skin, brain, head, and minced pork, respectively. The realized gain in different environments corresponds to the desired gain of implantable antennas in the ISM band [36]. Furthermore, the E- and H-plane gain patterns were omnidirectional in the HSP.

The implantable antenna uses electromagnetic (EM) waves to transfer biotelemetric data. Therefore, considering SAR is crucial for measuring the EM power absorbed by the body per unit mass. According to the two IEEE standards, IEEE C95.1−1999 and IEEE C95.1−2005, the safety limits are 1.6 and 2 W/kg averaged over 1 and 10 g of human tissues, respectively. By setting the input power to 1 W, a peak SAR value of 350.81 W/kg (1 g) was obtained at 2.45 GHz (Fig. 13). To maintain the radiator under the safety limit, the net input power to the antenna should not exceed 4.56 mW, as it is the critical value at which the peak SAR value reaches the critical limit of 1.6 W/kg. The results of the safety analysis performed using the proposed implantable antenna listed in Table 3 indicate that the SAR is not an issue of concern.

**TABLE 3.** 1-g peak special SAR and maximum allowable power at ISM (2.45 GHz) band.

| Body phantoms | Peak SAR (W/kg) | Max. allowable input power (mW) |
|---|---|---|
| Skin tissue | 289.76 | 5.52 |
| Head tissue | 350.81 | 4.56 |

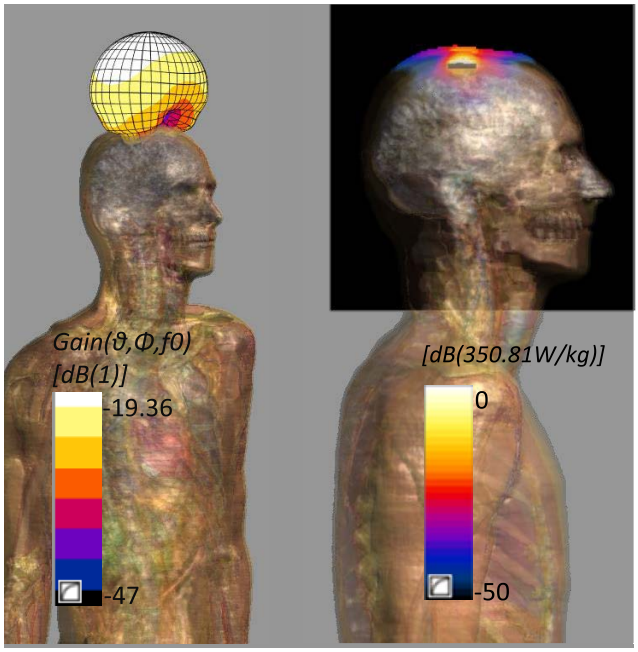


**FIGURE 13.** SAR and gain of the proposed antenna.

## IV. LINK BUDGET ANALYSIS OF THE PROPOSED ANTENNA

A link budget analysis was performed to exchange physiological data between the implantable antenna and the external controller. The development of a robust and reliable link based on link budget calculations proves a challenge because of the presence of different types of attenuations, including cable and connector losses, path loss, and antenna losses (mismatch and material) [37]. For a stable biotelemetric link, the difference between the antenna power ($A_P$) and the required power ($R_P$), known as the link margin, should be greater than 0. However, this study considered a link margin of 10 dB for improved reliability. The required antenna power is calculated as follows:

$$R_P = \frac{E_b}{N_o} + KT + B_r, \tag{1}$$

where $E_b/N_o$ is the ideal phase-shift keying with a value of 9.6 dB, $K$ is the Boltzmann's constant ($1.38 \times 10^{-23}$), $T_o$ is the temperature ($K$), and $B_r$ is the bit rate in Kbps/Mbps. The important parameters in the calculation of the link budget are listed in Table 4. According to IEEE safety limits, the input power to the implantable device is restricted to 25 $\mu$W (−16 dBm). To ensure safety, the effective isotropic radiated power (EIRP) of the implanted antenna must be less than or equal to $EIRP_{max}$. The $EIRP_{max}$ for the ISM (2.45 GHz)

**TABLE 4. Link budget parameters of the proposed antenna).**

| Symbol | Quantity | Bit Rate (200 Kbps) |
|---|---|---|
| $P_a$ | Transmitter power (dBm) | $-16$ |
| $N_o$ | Noise power density:(dB/Hz) | $-20.93$ |
| $T$ | Temperature (Kelvin) | 273 |
| $f$ | Resonating frequency | 2.45 GHz |
| $G_a$ | Transmitter antenna gain (dBi) | Tissue dependent |
| $G_b$ | Receiver antenna gain (dBi) | 2.15 |
| $L$ | Free space loss (dB) | Distance dependent |
| $A_P$ | Available power (dB) | Distance dependent |
| $R_P$ | Required power (dB) | $-155.9$ |
| $A_p - R_p$ | Margin (dB) | Fig. 18 |

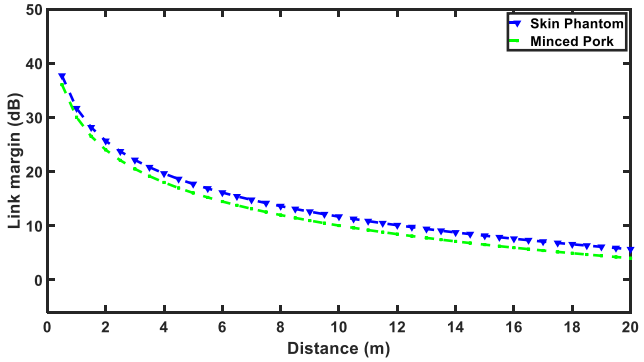


**FIGURE 14. Link budget at ISM (2.45 GHz) band.**

band is 20 dBm [38]. In this study, the transmitted power $P_a$ was assumed to be -16 dBm. Similarly, a bit rate $B_r$ of 200 Kbps was assumed to ensure an extended battery life to drive the circuitry of the implantable device integrated with the antenna. The available power of the proposed antenna is calculated as

$$A_P(dB) = P_a + G_a + G_b - L, \tag{2}$$

where $P_a$ is the transmitted power (dBm), $G_a$ represents the gain (dBi) of the transmitter antenna, $G_b$ is the receiver gain (dBi), and $L_f$ is the free space loss (dB). For the proposed antenna, $G_a$ is the tissue-dependent gain, and $G_b$ is the constant gain (2.15 dBi) of an ideal dipole receiver. The free-space loss ($L$) is calculated as

$$L(dB) = 20log(\frac{4\pi d}{\lambda}). \tag{3}$$

The distance versus link margin graph is shown in Fig. 13. Evidently, a maximum communication range of 12 m is achieved at a bitrate of 200 kbps and input power of $-16$ dBm.

## V. CONCLUSION

This paper presented a novel ultra-wideband implantable antenna operating at 2.45 GHz for biomedical applications, particularly for skin implantation. A shorting pin and rectangular and circular slots were added to the ground plane in addition to patches for antenna miniaturization. Several key parameters were analyzed to obtain the final design with a volume of only 9.8 mm$^3$ in the ISM band. Moreover, the SAR analysis results indicate that the proposed antenna can be safely implanted in patients. The antenna exhibits several essential features, including ultra-compact size, ultra-wide bandwidth, perfect impedance matching, high gain, omnidirectional radiation pattern, patient safety, and biotelemetric capability. Furthermore, the results of the comparative analysis demonstrate that proposed antenna offers superior performance compared to existing state-of-the-art implantable antennas.

## ACKNOWLEDGMENT

*(Naeem Abbas and Syed Ahson Ali Shah are co-first authors.)*

## REFERENCES

[1] I. A. Shah, M. Zada, and H. Yoo, "Design and analysis of a compact-sized multiband spiral-shaped implantable antenna for scalp implantable and leadless pacemaker systems," *IEEE Trans. Antennas Propag.*, vol. 67, no. 6, pp. 4230–4234, Jun. 2019.

[2] C. Liu, Y.-X. Guo, and S. Xiao, "Circularly polarized helical antenna for ISM-band ingestible capsule endoscope systems," *IEEE Trans. Antennas Propag.*, vol. 62, no. 12, pp. 6027–6039, Dec. 2014.

[3] S. M. Huang, M. R. Tofighi, and A. Rosen, "Considerations for the design and placement of implantable annular slot antennas for intracranial pressure monitoring devices," *IEEE Antennas Wireless Propag. Lett.*, vol. 14, pp. 1514–1517, 2015.

[4] C. Liu, Y. X. Guo, R. Jegadeesan, and S. Xiao, "*In vivo* testing of circularly polarized implantable antennas in rats," *IEEE Antennas Wireless Propag. Lett.*, vol. 14, pp. 783–786, 2015.

[5] A. Kumar, D. Chaturvedi, and S. I. Rosaline, "Design of antenna-multiplexer for seamless on-body Internet of Medical Things (IoMT) connectivity," *IEEE Trans. Circuits Syst. II, Exp. Briefs*, early access, Jun. 26, 2022, doi: 10.1109/TCSII.2022.3170513.

[6] D. Chaturvedi, A. Kumar, and S. Raghavan, "Wideband HMSIW-based slotted antenna for wireless fidelity application," *IET Microw., Antennas Propag.*, vol. 13, no. 2, pp. 258–262, Feb. 2019.

[7] A. A. Althuwayb, M. J. Al-Hasan, A. Kumar, and D. Chaturvedi, "Design of half-mode substrate integrated cavity inspired dual-band antenna," *Int. J. RF Microw. Comput.-Aided Eng.*, vol. 31, no. 2, 2021, Art. no. e22520.

[8] A. Iqbal, M. Al-Hasan, I. B. Mabrouk, and M. Nedil, "A compact implantable MIMO antenna for high-data-rate biotelemetry applications," *IEEE Trans. Antennas Propag.*, vol. 70, no. 1, pp. 631–640, Jan. 2022.

[9] A. J. Alazemi and A. Iqbal, "A high data rate implantable MIMO antenna for deep implanted biomedical devices," *IEEE Trans. Antennas Propag.*, vol. 70, no. 2, pp. 998–1007, Feb. 2022.

[10] A. Iqbal, M. Al-Hasan, I. Mabrouk, and M. Nedil, "Scalp-implantable MIMO antenna for high-data-rate head implants," *IEEE Antennas Wireless Propag. Lett.*, vol. 20, no. 12, pp. 2529–2533, Dec. 2021.

[11] H. Li, Y. X. Guo, C. Liu, S. Xiao, and L. Li, "A miniature-implantable antenna for MedRadio-band biomedical telemetry," *IEEE Antennas Wireless Propag. Lett.*, vol. 14, pp. 1176–1179, 2015.

[12] A. Rahman, M. T. Islam, M. J. Singh, S. Kibria, and M. Akhtaruzzaman, "Electromagnetic performances analysis of an ultra-wideband and flexible material antenna in microwave breast imaging: To implement a wearable medical bra," *Sci. Rep.*, vol. 6, no. 1, pp. 1–11, Dec. 2016.

[13] R. S. Alrawashdeh, Y. Huang, M. Kod, and A. A. B. Sajak, "A broadband flexible implantable loop antenna with complementary split ring resonators," *IEEE Antennas Wireless Propag. Lett.*, vol. 14, pp. 1506–1509, 2015.

[14] M. Kod, J. Zhou, Y. Huang, M. Stanley, M. N. Hussein, A. P. Sohrab, R. Alrawashdeh, and G. Wang, "Feasibility study of using the housing cases of implantable devices as antennas," *IEEE Access*, vol. 4, pp. 6939–6949, 2016.

[15] S. Kim and H. Shin, "An ultra-wideband conformal meandered loop antenna for wireless capsule endoscopy," *J. Electromagn. Eng. Sci.*, vol. 19, no. 2, pp. 101–106, Apr. 2019.

[16] R. Alrawashdeh, "Implantable antennas for biomedical applications," Ph.D. dissertation, Dept. Elect. Eng. Electron., Univ. Liverpool, Liverpool, U.K., 2015.

[17] Y. Fan, J. Huang, T. Chang, and X. Liu, "A miniaturized four-element MIMO antenna with EBG for implantable medical devices," *IEEE J. Electromagn., RF, Microw. Med. Biol.*, vol. 2, no. 4, pp. 226–233, Dec. 2018.
[18] R. Lesnik, N. Verhovski, I. Mizrachi, B. Milgrom, and M. Haridim, "Gain enhancement of a compact implantable dipole for biomedical applications," *IEEE Antennas Wireless Propag. Lett.*, vol. 17, no. 10, pp. 1778–1782, Oct. 2018.
[19] Z.-J. Yang, L. Zhu, and S. Xiao, "An implantable circularly polarized patch antenna design for pacemaker monitoring based on quality factor analysis," *IEEE Trans. Antennas Propag.*, vol. 66, no. 10, pp. 5180–5192, Oct. 2018.
[20] M. Zada and H. Yoo, "A miniaturized triple-band implantable antenna system for bio-telemetry applications," *IEEE Trans. Antennas Propag.*, vol. 66, no. 12, pp. 7378–7382, Dec. 2018.
[21] Y. Cho and H. Yoo, "Miniaturised dual-band implantable antenna for wireless biotelemetry," *Electron. Lett.*, vol. 52, no. 12, pp. 1005–1007, May 2016.
[22] X. Y. Liu, Z. T. Wu, Y. Fan, and E. M. Tentzeris, "A miniaturized CSRR loaded wide-beamwidth circularly polarized implantable antenna for subcutaneous real-time glucose monitoring," *IEEE Antennas Wireless Propag. Lett.*, vol. 16, pp. 577–580, 2016.
[23] S. Das and D. Mitra, "A compact wideband flexible implantable slot antenna design with enhanced Gain," *IEEE Trans. Antennas Propag.*, vol. 66, no. 8, pp. 4309–4314, Aug. 2018.
[24] Z.-J. Yang, L. Zhu, and S. Xiao, "An implantable wideband circularly polarized microstrip patch antenna via two pairs of degenerate modes," *IEEE Access*, vol. 7, pp. 4239–4247, 2019.
[25] I. Gani and H. Yoo, "Multi-band antenna system for skin implant," *IEEE Microw. Wireless Compon. Lett.*, vol. 26, no. 4, pp. 294–296, Apr. 2016.
[26] L.-J. Xu, Y.-X. Guo, and W. Wu, "Miniaturized dual-band antenna for implantable wireless communications," *IEEE Antennas Wireless Propag. Lett.*, vol. 13, pp. 1160–1163, 2014.
[27] C. Liu, Y.-X. Guo, and S. Xiao, "Capacitively loaded circularly polarized implantable patch antenna for ISM band biomedical applications," *IEEE Trans. Antennas Propag.*, vol. 62, no. 5, pp. 2407–2417, May 2014.
[28] J. Blauert, Y.-S. Kang, and A. Kiourti, "*In vivo* testing of a miniature 2.4/4.8 GHz implantable antenna in postmortem human subject," *IEEE Antennas Wireless Propag. Lett.*, vol. 17, no. 12, pp. 2334–2338, Dec. 2018.
[29] F.-J. Huang, C.-M. Lee, C.-L. Chang, L.-K. Chen, T.-C. Yo, and C.-H. Luo, "Rectenna application of miniaturized implantable antenna design for triple-band biotelemetry communication," *IEEE Trans. Antennas Propag.*, vol. 59, no. 7, pp. 2646–2653, Jul. 2011.
[30] A. Kiourti, M. Christopoulou, and K. S. Nikita, "Performance of a novel miniature antenna implanted in the human head for wireless biotelemetry," in *Proc. IEEE Int. Symp. Antennas Propag. (APSURSI)*, Jul. 2011, pp. 392–395.
[31] H. Li, Y.-X. Guo, and S.-Q. Xiao, "Broadband circularly polarised implantable antenna for biomedical applications," *Electron. Lett.*, vol. 52, no. 7, pp. 504–506, Mar. 2016.
[32] C. G. L. Khoo, B. Brox, R. Norrhede, and F. H. J. Maurer, "Effect of copper lamination on the rheological and copper adhesion properties of a thermotropic liquid crystalline polymer used in PCB applications," *IEEE Trans. Compon., Packag., Manuf. Technol.*, vol. 20, no. 3, pp. 219–226, Jul. 1997.
[33] N. R. Rishani, R. M. Shubair, and G. Aldabbagh, "On the design of wearable and epidermal antennas for emerging medical applications," in *Proc. Sensors Netw. Smart Emerg. Technol. (SENSET)*, Sep. 2017, pp. 1–4.
[34] A. Kiourti and K. S. Nikita, "A review of implantable patch antennas for biomedical telemetry: Challenges and solutions [wireless corner]," *IEEE Antennas Propag. Mag.*, vol. 54, no. 3, pp. 210–228, Jun. 2012.
[35] Y. Cho and H. Yoo, "Miniaturised dual-band implantable antenna for wireless biotelemetry," *Electron. Lett.*, vol. 52, no. 12, pp. 1005–1007, May 2016.
[36] Z. Duan, Y.-X. Guo, M. Je, and D.-L. Kwong, "Design and *in vitro* test of a differentially fed dual-band implantable antenna operating at MICS and ISM bands," *IEEE Trans. Antennas Propag.*, vol. 62, no. 5, pp. 2430–2439, May 2014.
[37] A. Kiourti and K. S. Nikita, "Miniature scalp-implantable antennas for telemetry in the MICS and ism bands: Design, safety considerations and link budget analysis," *IEEE Trans. Antennas Propag.*, vol. 60, no. 8, pp. 3568–3575, Aug. 2012.
[38] A. Basir and H. Yoo, "Efficient wireless power transfer system with a miniaturized quad-band implantable antenna for deep-body multitasking implants," *IEEE Trans. Microw. Theory Techn.*, vol. 68, no. 5, pp. 1943–1953, May 2020.

**NAEEM ABBAS** received the B.Sc. degree in telecommunication engineering from the University College of Engineering and Technology (UCET), The Islamia University of Bahawalpur, Pakistan, in 2018, and the M.Sc. degree in telecommunication engineering from the University of Engineering and Technology (UET), Taxila, Pakistan, in 2021. He is currently a Registered Member of Pakistan Engineering Council (PEC). He is also working on implantable antennas and systems, passive chipless RFID tags, wireless power transfer, wireless communication, the Internet of Things (IoT), and image processing.

**SYED AHSON ALI SHAH** (Graduate Student Member, IEEE) received the B.Sc. degree in telecommunication engineering from the University of Engineering & Technology, Mardan, Pakistan, in 2015. He is currently pursuing the M.S. leading to Ph.D. degree in electronic engineering with the Applied Bioelectronics Laboratory, Hanyang University, Seoul, South Korea, under the supervision of Dr. Hyoungsuk Yoo.

He has (co)authored several IEEE TRANSACTIONS, journals, and conference papers. His research interests include implantable antennas and systems, implant safety, wireless power transfer to biomedical devices, implant safety, sensors integrated telemetric stents, reconfigurable antenna, and metamaterial-based antenna systems.

Mr. Ahson has received IETE MN SAHA Memorial Award and Gold Medal for best Application-Oriented Paper, in 2018. He has also received Bronze Paper Award at IEEE Student Paper Contest, Seoul, in 2019. He received another Bronze Paper Award at IEEE Student Paper Contest, Seoul, in 2021. He has also won 3rd Best Student Paper Award in 2021 Competition arranged by the Korean Institute of Electromagnetic Engineering & Science (KIEES). He has been a Registered Engineer with Pakistan Engineering Council (PEC), Pakistan, since 2016. He is also serving as a Reviewer for IEEE TRANSACTIONS IN ANTENNAS AND PROPAGATION, IEEE TRANSACTIONS ON INDUSTRIAL ELECTRONICS, IEEE ACCESS, *International Journal of RF and Microwave Computer-Aided Engineering*, and *SN Applied Sciences*.

**ABDUL BASIR** (Member, IEEE) was born in Khyber Pukhtoonkhwa, Pakistan, in 1989. He received the B.Sc. degree in telecommunication engineering from the University of Engineering & Technology, Peshawar, Pakistan, in 2015, and the Ph.D. degree in electronic engineering from Hanyang University, South Korea, in 2021. Since September 2021, he has been working as a Postdoctoral Researcher with the AB-Laboratory, Hanyang University. His research interests include implantable antennas and systems, biomedical circuits, wearable antennas, MIMO communication, metamaterial, dielectric resonator antennas, reconfigurable antennas, long range wireless power transfer, and wireless charging of biomedical implants. He was awarded Silver Prize for the best student paper awards in Student Paper Contests 2018 and 2019, IEEE Seoul Section. His collaborated paper was awarded with Best Paper Award 2019 by IEEE AP/MTT/EMC Joint Chapter Malaysia. He is also awarded with Third Prize for the Best Student Paper Completion 2018 by the Korea Communications Agency (KCA) and the Korean Institute of Electromagnetic Engineering & Science (KIEES).

**ZUBAIR BASHIR** received the B.Sc. degree in telecommunication engineering from the University of Engineering and Technology, Taxila, Pakistan, in 2019, where he is currently pursuing the M.Sc. degree with the Telecommunication Engineering Department. He joined the ACTSENA Research Group, University of Engineering and Technology, Taxila. His research interests include implantable antennas, meta-material, multiple-input and multiple-output (MIMO) systems, and reconfigurable antennas.

**ADEEL AKRAM** received the B.S. degree in electrical engineering from the University of Engineering and Technology at Lahore (CE and ME Campus), Lahore, Pakistan, in 1995, the M.S. degree in computer engineering from the National University of Science and Technology, Rawalpindi, Pakistan, in 2000, and the Ph.D. degree from the University of Engineering and Technology, Taxila, Taxila, Pakistan, in 2007. He is currently the Dean of the Faculty of Telecommunication and Information Engineering, University of Engineering and Technology, Taxila. His research interests include the Internet of Things, pervasive computing, wireless communications, broadband networking, and routing.

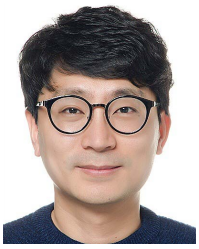

**HYOUNGSUK YOO** (Senior Member, IEEE) received the B.Sc. degree in electrical engineering from Kyungpook National University, Daegu, South Korea, in 2003, and the M.Sc. and Ph.D. degrees in electrical engineering from the University of Minnesota, Minneapolis, MN, USA, in 2006 and 2009, respectively. In 2009, he joined the Center for Magnetic Resonance Research, University of Minnesota, as a Postdoctoral Associate. In 2010, he joined Cardiac Rhythm Disease Management, Medtronic, MN, USA, as a Senior EM/MRI Scientist. From 2011 to 2018, he was an Associate Professor with the Department of Biomedical Engineering, School of Electrical Engineering, University of Ulsan, Ulsan, South Korea. Since 2018, he has been an Associate Professor with the Department of Biomedical Engineering, Hanyang University, Seoul, South Korea. He has been the CEO of E2MR, a startup company, since 2017. His current research interests include electromagnetic theory, numerical methods in electromagnetics, metamaterials, antennas, implantable devices, and magnetic resonance imaging in high-magnetic field systems. He was awarded Third Prize for the Best Student Paper at the 2010 IEEE Microwave Theory and Techniques Society International Microwave Symposium.